DAMAGE PARAMETERS FOR NON-METALS IN A HIGH ENERGY NEUTRON ENVIROMENT

G. F. Dell, H. C. Berry, O. W. Lazareth, and A. N. Goland

Brookhaven National Laboratory*
Upton, New York 11973, U.S.A.

ABSTRACT

Simulation of radiation damage induced in monatomic and binary non-metals by FMIT and fusion neutrons is described. Damage produced by elastic scattering of recoil atoms and by ionization-assisted processes has been evaluated using the damage program DON. Displacement damage from gamma rays has been evaluated by using the technique of Oen and Holmes. A comparison of damage for an anticipated FMIT radiation environment generated by a coupled n-γ transport calculations and a fusion spectrum is made. Gamma-induced displacement damage is sufficiently small that it is dominated by neutron-induced recoil processes. Ionization-assisted displacements may be important depending upon the ionization cross section of the particular non-metal under consideration.

INTRODUCTION

A realistic materials development program for fusion reactors requires the ability to expose samples to environments similar to that in a fusion reactor. The FMIT facility at HEDL will provide a means for performing needed irradiations. However, the volume in FMIT over which the neutron flux exceeds $1.0 \cdot 10^{15}$ n/cm^2·s will be modest ($\sim$10 cm^3), whereas the number of samples to be irradiated will be large and many samples will have to be exposed to a high fluence ($\geq 10^{22}$ n/cm^2). Even in the highest flux region of the FMIT, irradiations lasting a year will be required, and there will most likely be a backlog of samples to irradiate. Therefore it is desirable to expedite the test program by identifying promising materials prior to irradiation. It is also desirable to compare anticipated results from materials exposed to an FMIT radiation environment with the corresponding anticipated results for materials

*Supported by the U.S. Dept. of Energy.

exposed to a fusion reactor environment in order to ascertain whether the results are equivalent. The different nature of the flux spectra coupled with the reasons previously stated justifies a program to calculate expected damage to materials exposed to high fluences of neutrons and gamma rays.

The understanding of processes governing radiation damage in non-metals is an important aspect of the special materials development program for fusion reactors. Some typical uses of non-metals include use in the first wall, as insulators for neutral beam injectors, as insulators in power supplies, and in magnets. In this paper the status of our program in simulating damage in insulator materials is reported. Evaluations have been made for a hypothetical first-wall spectrum as well as for the neutron-gamma ray environment anticipated for the FMIT facility. Similarities and differences are noted as are limitations introduced by incomplete knowledge of cross sections and displacement energies.

FMIT FLUX CHARACTERIZATION

The FMIT radiation environment was generated by using the MORSE Monte-Carlo transport code to perform coupled n-γ transport calculations for a problem having geometry similar to that of an FMIT test facility. This geometry is shown in Fig. 1. A test module containing samples is positioned immediately downstream of a lithium target. The test module is 30 cm wide, 20 cm high, and 20 cm deep, and it is filled uniformly with quarter-density iron. These dimensions were selected arbitrarily and differ somewhat from the 15 cm depth of half-density iron used in calculations at HEDL. The fluxes are slightly different for the two geometries, but the conclusions we reach are unaffected by these flux differences.

Neutrons are generated in a volume 3 cm wide, 1 cm high, and 2 cm thick that corresponds to the dimensions of the lithium target. The deuteron beam is assumed to have uniform intensity along the 3 cm width of the target and to have a gaussian profile in the vertical direction. Neutrons are generated randomly with depth in the target. The energy of the deuteron at the point of interaction is obtained from the range-energy relation for 35 MeV deuterons in lithium. The initial direction and energy of each neutron is generated randomly using Serber's [1] transparent nucleus model as well as the evaporation model. The ratio between stripping and evaporation neutrons was adjusted to give a reasonable fit to the neutron spectra measured by Saltmarsh et al. [2]

The high-energy neutron cross sections of Alsmiller and Barish [3] were used in performing the transport calculations. These cross sections extend to 60 MeV, but only eleven materials, including high-density concrete, are included in the set. As lithium is not among them, the lithium target was assumed to be transparent to neutrons.

The neutron and gamma ray fluxes were determined at several points along the central axis of the test module. Flux characterizations were performed for the test module located within a 5' × 6' × 8' cave having 1 m thick walls of high density concrete.

The fluxes generated by MORSE have units of flux per primary neutron. Conventional units are obtained by multiplying the MORSE fluxes by the neutron yield from 35 MeV deuterons in a thick lithium target. A value of $2.75 \cdot 10^{17}$ n/Coulomb has been deduced by interpolating between the yield at 40 MeV measured by Saltmarsh et al. [2] and the yields at lower energies [4]. The FMIT spectrum at a distance of 4 cm from the lithium target and the fusion spectrum used in the present evaluations appear in Fig. 2.

DAMAGE ANALYSIS

The high-energy neutron cross sections of Alsmiller and Barish were used for characterizing the radiation environment in the test module, and then ENDF/B-V cross sections were used with the damage program DON [5] to evaluate damage parameters in various materials. For the FMIT neutron spectrum used in the present evaluation, 38% of the neutrons have energy greater than 14.9 MeV, and 21% have energy above 20 MeV. For those neutrons having energy above 20 MeV, a high-energy extrapolation of the cross section is made by the DON program.

The neutron and gamma-ray flux spectra generated during the transport calculation were used to evaluate neutron-induced recoil atom damage, gas production rates, recoil damage initiated by energetic electrons produced by gamma-rays, and damage induced by a particular ionization process involving L shell ionization of atoms by primary knock-on atoms. These types of damage are discussed below.

Neutron-Induced Recoil Damage

For monatomic materials we have used the Robinson [6] form of the Lindhard function L(T) to relate recoil energy T to damage energy in the DON program, and we have used the Kinchin-Pease relation to relate damage energy to displacements $\nu(T)$

$$\nu(T) = \frac{0.8\,T\,L(T)}{2E_d} \qquad (1)$$

where E_d is the displacement threshold energy.

For multicomponent materials the division of damage energy between the different species of atoms is complicated, and different atomic species can have different displacement energies. Parkin and Coulter [7] have obtained numerical solutions to the integro-differential equation of Lindhard [8] for several binary materials of interest to us. They have generated tables of displacement functions for Al_2O_3, Si_3N_4, and CaO. These tables

have been incorporated in the damage program DON and serve as lookup tables for relating displacements to PKA energy.

Evaluation of displacement cross sections for a binary material requires four separate calculations; displacements of each species of atom by each species of PKA must be evaluated. As an example, for Al_2O_3, it is necessary to determine the number of oxygen atoms displaced by aluminum PKA's, n(Al,O), as well as by oxygen PKA's, n(O,O). The results are then combined according to the atomic fraction of each species of PKA:

$$n(Al) = 0.4\ n(Al,Al) + 0.6\ n(O,Al)$$
$$n(O) = 0.4\ n(Al,O) + 0.6\ n(O,O). \qquad (2)$$

The spectrum-averaged displacement cross sections for Al_2O_3 and Si_3N_4 have been evaluated for the FMIT and fusion reactor first wall spectra of Fig. 2, and the results are listed in Table I.

TABLE I

Spectrum Averaged Displacement and Gas Production Cross Sections for Al_2O_3 and Si_3N_4

Al_2O_3			Si_3N_4		
	FMIT	FUSION		FMIT	FUSION
$\bar{\sigma}_d$(Al) (b/atom)	1111.5	723.6	$\bar{\sigma}_d$(Si) (b/atom)	392.9	220.1
$\bar{\sigma}_d$(O) (b/atom)	428.8	280.1	$\bar{\sigma}_d$(N) (b/atom)	452.4	255.0
$\bar{\sigma}_H$ (mb/atom)	39.0	18.5	$\bar{\sigma}_H$ (mb/atom)	156.0	75.2
$\bar{\sigma}_{He}$ (mb/atom)	53.6	33.0	$\bar{\sigma}_{He}$ (mb/atom)	151.0	61.1
H/dpa(Al) (appm)	35.1	25.5	H/dpa(Si) (appm)	397.0	341.7
He/dpa(Al) (appm)	53.6	45.6	He/dpa(N) (appm)	384.3	277.6

The large difference in displacement cross sections for aluminum and oxygen in Al_2O_3 is a direct result of the different displacement energies used in the evaluation. The displacement energies were measured by Pells and Phillips [9] with a HVEM, and were found to be 18 and ~75 eV for aluminum and oxygen, respectively. A displacement energy of 60 eV was used for both silicon and nitrogen in Si_3N_4 in the absence of experimental values.

Gas Production

Spectrum-averaged cross sections for hydrogen and helium production are evaluated by the damage program DON. The spectrum-

averaged gas cross sections for Al_2O_3 and Si_3N_4 have been obtained by weighting the contribution from each species according to its atomic percentage in the compound.

The He/dpa ratio can vary with position in the test module. In Fig. 3 the dependence of the He/dpa ratio in silicon upon depth in the module and upon average density of the module is compared to the He/dpa ratio for the fusion spectrum. The decrease of the He/dpa ratio with increasing material thickness results from a decrease in the average energy of the neutron spectrum. As there are many high-energy neutrons in the high flux region near the lithium target, neutron cross sections above 20 MeV are needed for calculations of He/dpa ratios in this important region.

Gamma Ray-Induced Displacements

Displacement cross sections for recoil atom damage initiated by energetic electrons that are produced during gamma-ray interactions have been evaluated using the method of Oen and Holmes [10] for Compton and photoelectric processes and of Cahn [11] for the pair-production process. Their calculations, made for gamma-ray energies up to 5 and 7 MeV, respectively, have been extended to 15 MeV. The displacement functions of Parkin and Coulter were used to obtain the displacement cross sections for aluminum and oxygen in Al_2O_3 exposed to the FMIT gamma-ray spectrum shown in Fig. 4. This spectrum was generated for a point 0.5 cm from the lithium target and represents the most intense gamma-ray flux in the test module. The gamma-ray flux, average energy, and spectrum averaged displacement cross sections for aluminum and oxygen in Al_2O_3 are listed in Table II.

TABLE II

Gamma-ray Induced Damage in Al_2O_3

γ-Flux ($\gamma/cm^2 \cdot s$)	$3.0 \cdot 10^{14}$
$\bar{E}_\gamma$ (MeV)	1.83
$\bar{\sigma}_d^{\gamma}$(Al) barns/atom	0.90
$\bar{\sigma}_d^{\gamma}$(O) barns/atom	0.57

The spectrum-averaged cross sections for gamma-ray initiated recoil-atom damage in the test module is insignificant compared with neutron-initiated recoil-atom damage [9] while the gamma

heating at this position is $1.25 \cdot 10^{13}$ MeV/g·s. It is to be stressed that our present gamma-ray fluxes are probably low. The Alsmiller-Barish cross sections do not include gamma-ray production or gamma-ray downscatter for neutrons whose energies are above 14.9 MeV. Since nearly 40% of the neutrons in the FMIT spectrum of Fig. 2 have such energies, they have not contributed to the calculated spectrum of gamma rays. It is anticipated that inclusion of gamma production and downscatter for neutrons above 14.9 MeV would substantially increase the gamma-ray flux and the average energy of the gamma-ray spectrum. Moreover, the spectrum-averaged displacement cross section could easily increase due to this effect, although gamma-ray initiated displacements induced by energetic electrons should still be much smaller than neutron-induced recoil-atom displacements.

Ionization-Assisted Displacement Processes

A displacement mechanism involving ionization of atoms by a PKA, and subsequent repulsion between the PKA and the ionized atom has been described by Yarlagadda and Robinson [12].

The role of such ionization-assisted damage processes involving L-shell ionization of carbon and Al_2O_3 has been evaluated for the fusion spectrum and for the FMIT spectrum of Fig. 2. These calculations require a knowledge of the cross section for L-shell ionization of an atom by the recoil atom. Unfortunately, few experimental data exist for L-shell ionization in ion-atom collisions. Consequently, we have used the model of Fortner et al. [13] to evaluate cross sections of interest to us. The experimental data of Fortner et al. for L-shell ionization in Ar-Ar interactions were used to estimate the values of the parameters needed to evaluate L-shell ionization cross sections for Al-Al, Al-O, O-Al, and O-O interactions.

The ionization-assisted stopping cross section $S_I(T)$ was expressed by Yarlagadda and Robinson as:

$$S_I(T) = \sigma_I^L(T)\Delta E_d \tag{3}$$

where $\sigma_I^L(T)$ is the L-shell ionization cross section at energy T, and ΔE_d is the energy lost in displacing an atom.

The importance of the ionization-assisted mechanism was assessed by constructing functions, L'(T), similar to the Lindhard function, expressing the fraction of the total energy that is lost through ionization-assisted processes.

$$L'(T) = \frac{\sum_{T'=0}^{T} S_I(T)\Delta T'}{\sum_{T'=0}^{T} [S_n(T)+S_e(T)]\Delta T'} \tag{4}$$

where $S_n(T)$ and $S_e(T)$ are the Lindhard nuclear stopping cross section and the electronic stopping cross section, respectively.

The functions $L'(T)$ were incorporated in DON, and the displacement cross section was evaluated for each ion-atom combination.

The ionization-assisted displacement cross sections for carbon as well as for aluminum and oxygen in Al_2O_3 are listed in Table III along with the corresponding cross sections for neutron-induced damage.

TABLE III

Comparison of Spectrum Averaged Displacement Cross Sections for Ionization-Assisted and Neutron-Induced Recoil Atom Damage in Al_2O_3 and Carbon

$\bar{\sigma}_d$ (barns/atom)	Al_2O_3				CARBON	
	FMIT		FUSION		FMIT	FUSION
	Al	O	Al	O		
Ionization Assisted	79	201	37	94	1200	548
Recoil Atom	1112	429	724	280	730	642
$\frac{dpa(Ion)}{dpa(Recoil)}$	0.071	0.469	0.051	0.336	1.64	0.854

Based on these values it is concluded that ionization-assisted damage can be important in non-metals. At present our estimates of this type of damage are crude due largely to uncertainties in ionization cross sections and displacement energies, but these initial results indicate that further consideration of this mechanism is warranted for nonmetals.

CONCLUSIONS

Neutron-initiated recoil atom damage and ionization-assisted damage are coupled to the neutron cross sections through the primary knock-on atom. Gas production depends directly upon the hydrogen and helium production cross sections, and gamma-ray initiated damage depends upon gamma-ray production and downscatter probabilities. Hence any extensions of the neutron cross sections to energies above 20 MeV will have direct impact on our simulations. In addition, ionization cross sections for ion-atom inter-

interactions are needed as are displacement threshold energies for multicomponent materials.

REFERENCES

1. R. SERBER, "The Production of High Energy Neutrons by Stripping," Phys. Rev. 72, 1008 (1959).

2. M. J. SALTMARSH et al., "Characteristics of an Intense Neutron Source Based on the d+Be Reaction," Nucl. Inst. and Methods 145, 81 (1977).

3. R. G. ALSMILLER, JR. and J. BARISH, "Neutron-Photon Multigroup Cross Sections for Neutron Energies ≤60 MeV," Nucl. Sci. and Eng. 69, 378 (1979).

4. P. J. PERSIANI, W. BECKER, and J. DONAHUE, "Neutron Spectra and Basic Data Requirements for (d,Li) and (d,Be) Target Systems," Symposium on Neutron Cross Sections from 10-40 MeV, Brookhaven National Laboratory, May 3-5, 1977, BNL-NLS-50681, p. 151.

5. D. M. PARKIN and A. N. GOLAND, "Calculation of Radiation Effects as a Function of Incident Neutron Spectrum," Radiation Effects 28, 31 (1976).

6. M. T. Robinson, "The Energy Dependence of Neutron Radiation Damage in Solids," in Proc. Brit. Nucl. Energy Soc. Conf. on Nucl. Fusion Reactors, British Nuclear Energy Society, London (1970) p. 364.

7. D. M. PARKIN and C. A. COULTER, "Displacement Functions for Diatomic Materials," J. of Nucl. Materials 85 & 86, 611 (1979).

8. J. LINDHARD et al., "Integral Equations Governing Radiation Effects," Kgl. Dansk, Vedenskab. Selsk, Mat.-Fys. Medd. 33 #10 (1963).

9. G. P. PELLS and D. C. Phillips, "Radiation Damage of α-Al_2O_3 in the HVEM," J. of Nucl. Materials 80, 207 (1979).

10. O. S. OEN and D. K. HOLMES, "Cross Sections for Atomic Displacements in Solids by Gamma Rays," J. Appl. Phys. 30, 1289 (1959).

11. J. H. CAHN, "Irradiation Damage in Germanium and Silicon due to Electrons and Gamma Rays," J. Appl. Phys. 30, 1310 (1959).

12. B. S. YARLAGADDA and J. E. ROBINSON, "Assessment of Ionization-Assisted Damage Processes in CTR First-Wall Materials," J. of Nucl. Materials 63, 466 (1976).

13. R. J. FORTNER et al., "X-Ray Production in C^+-C Collisions in the Energy Range 20 keV to 1.5 MeV," Phys. Rev. 185, 164 (1969).

FIGURE CAPTIONS

Fig. 1 Geometry used for characterizing the neutron-gamma ray radiation environment in a FMIT irradiation cave with the MORSE transport code. A beam of 35 MeV deuterons (d BEAM) is incident on a volume (Li) representing the dimensions of the lithium target. The iron block test assembly consists of quarter-density iron.

Fig. 2 Neutron spectra used to assess radiation damage. The "First Wall" spectrum corresponds to a 1 MW/m^2 wall loading and has a total flux of $3.81 \cdot 10^{14}$ $n/cm^2 \cdot s$.

The "FMIT" spectrum corresponds to the neutron flux at a point on the beam axis 4 cm from the lithium target. Total flux is $1.56 \cdot 10^{15}$ $n/cm^2 \cdot s$.

Fig. 3 Dependence of the He/dpa rates upon the depth within the test assembly as well as on the average density of the test assembly.

Fig. 4 FMIT-gamma ray spectrum generated with MORSE for a point on the beam axis at a distance of 0.5 cm from the lithium target. HEDL-gamma ray spectrum generated at HEDL for a point on the beam axis and 0.25 cm from the target backing plate.

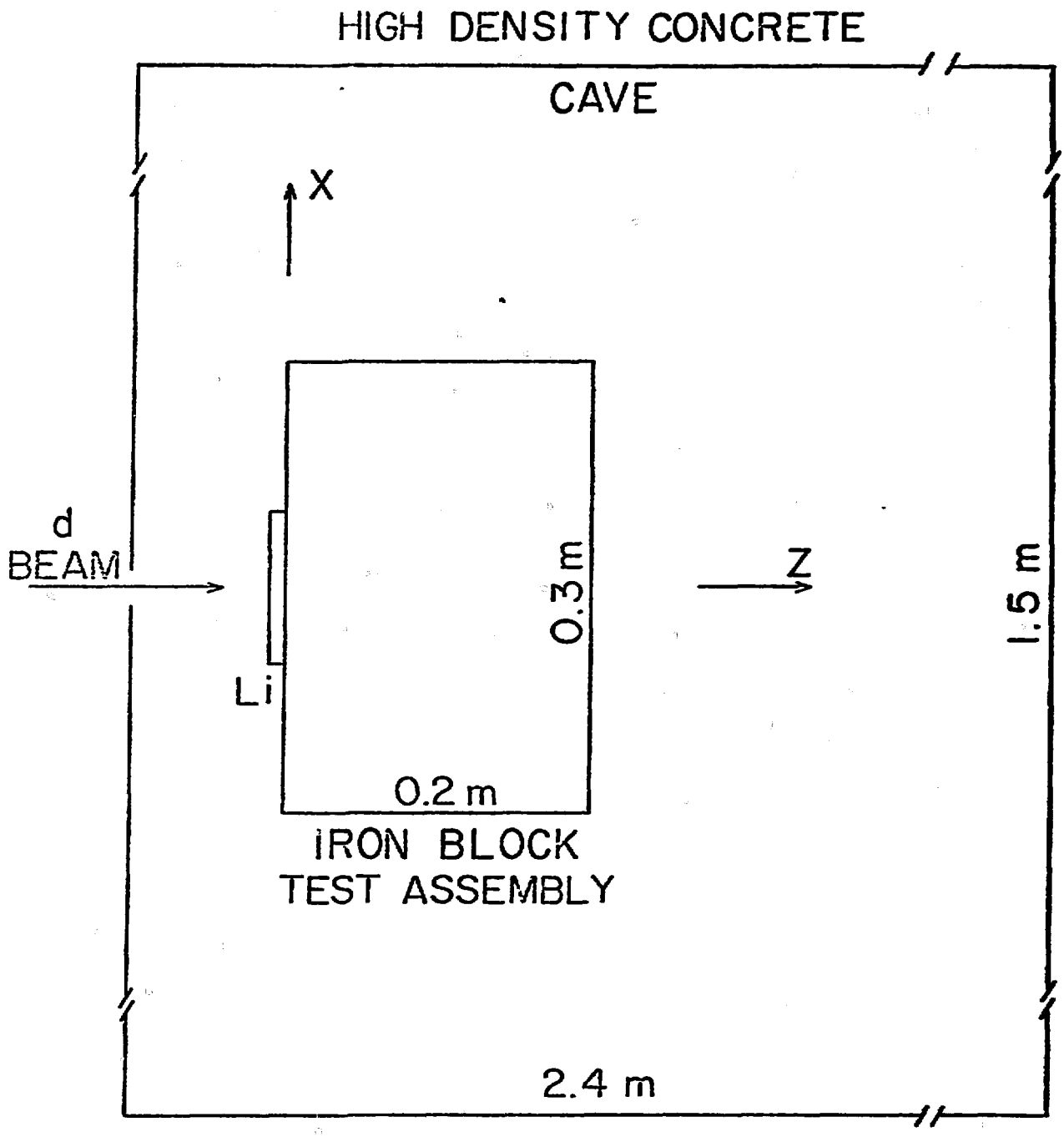
HIGH DENSITY CONCRETE
CAVE
X
d
BEAM
Z
0.3 m
1.5 m
Li
0.2 m
IRON BLOCK
TEST ASSEMBLY
2.4 m

FIGURE 1

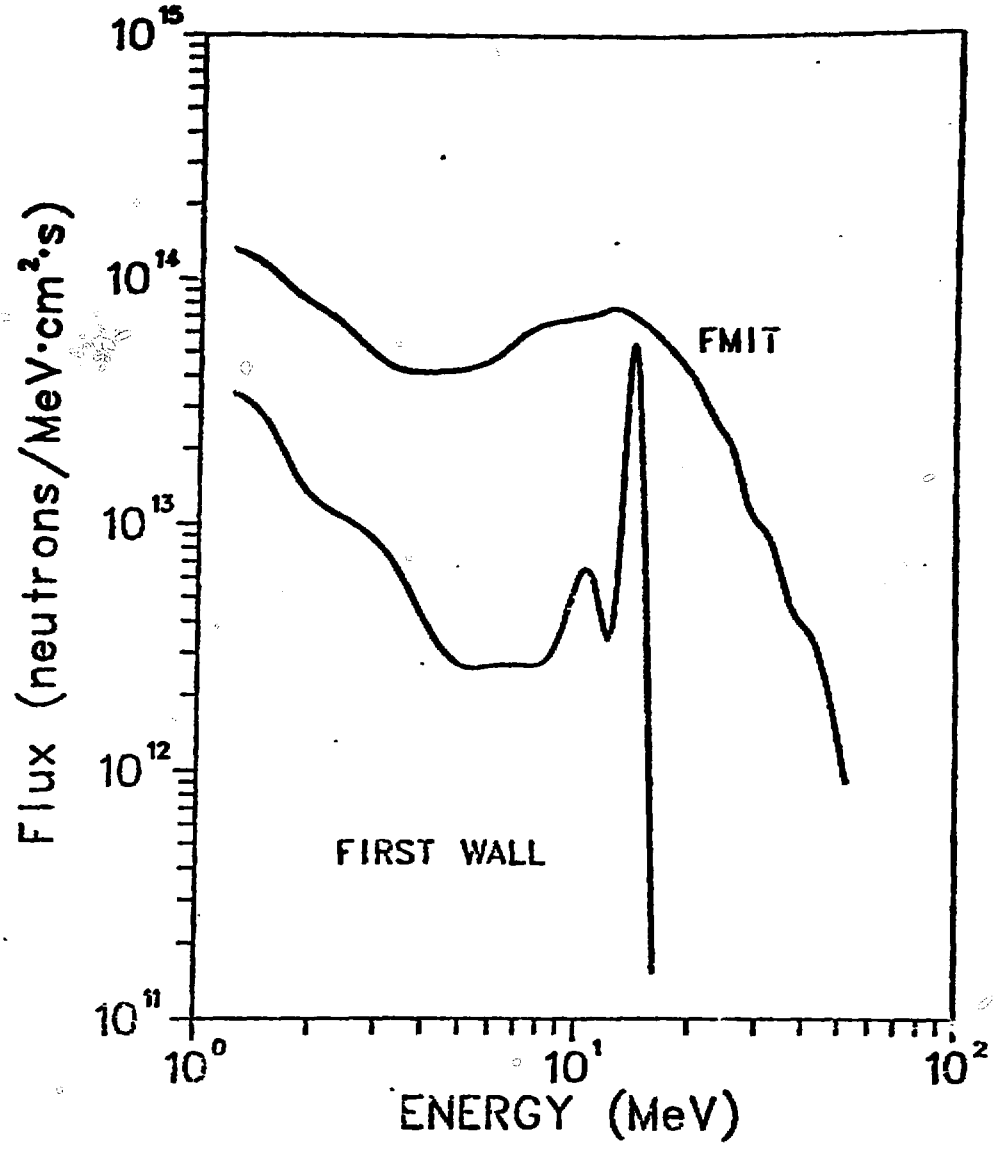
10^{15}
10^{14}
10^{13}
10^{12}
10^{11}
Flux (neutrons/MeV·cm²·s)
FMIT
FIRST WALL
10^{0}
10^{1}
10^{2}
ENERGY (MeV)

FIGURE 2

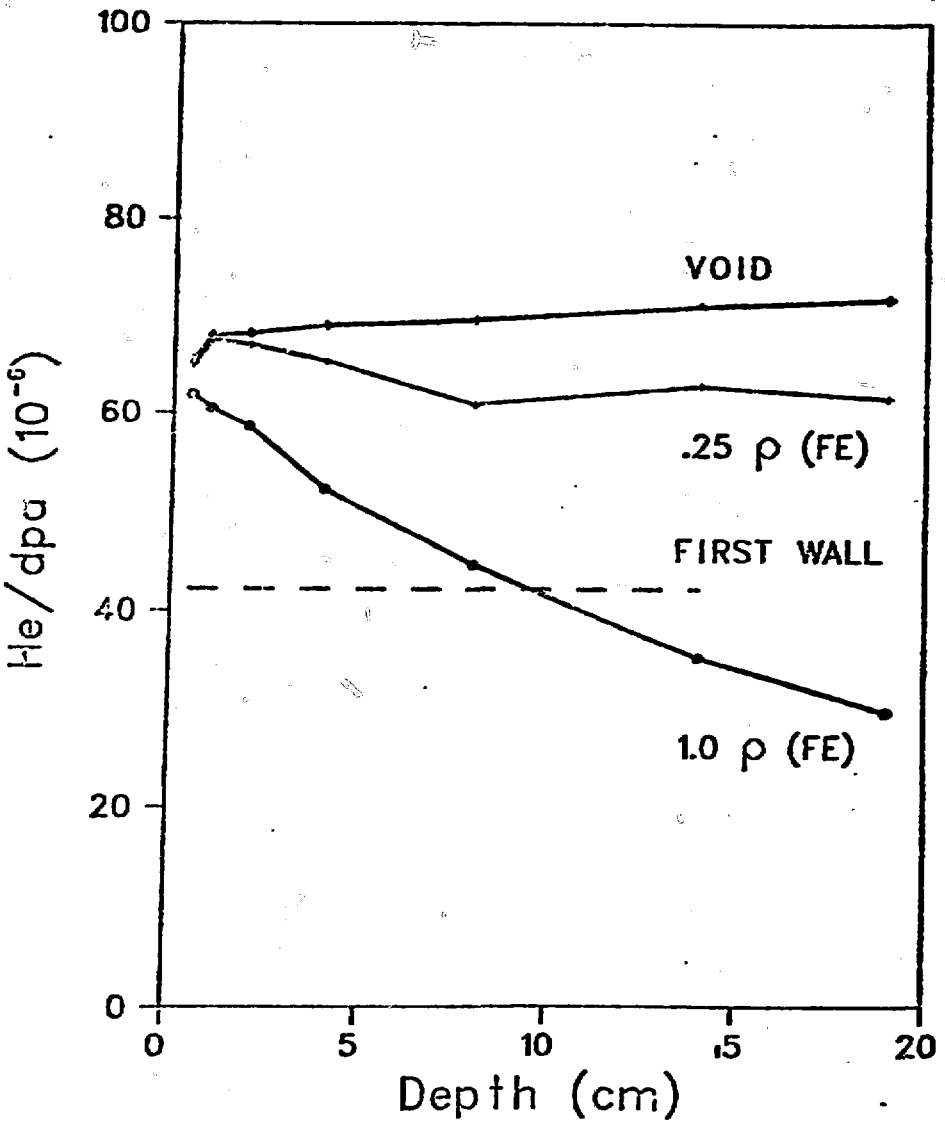
100
80
60
40
20
0
He/dpa (10^{-6})
VOID
.25 ρ (FE)
FIRST WALL
1.0 ρ (FE)
0
5
10
15
20
Depth (cm)

FIGURE 3

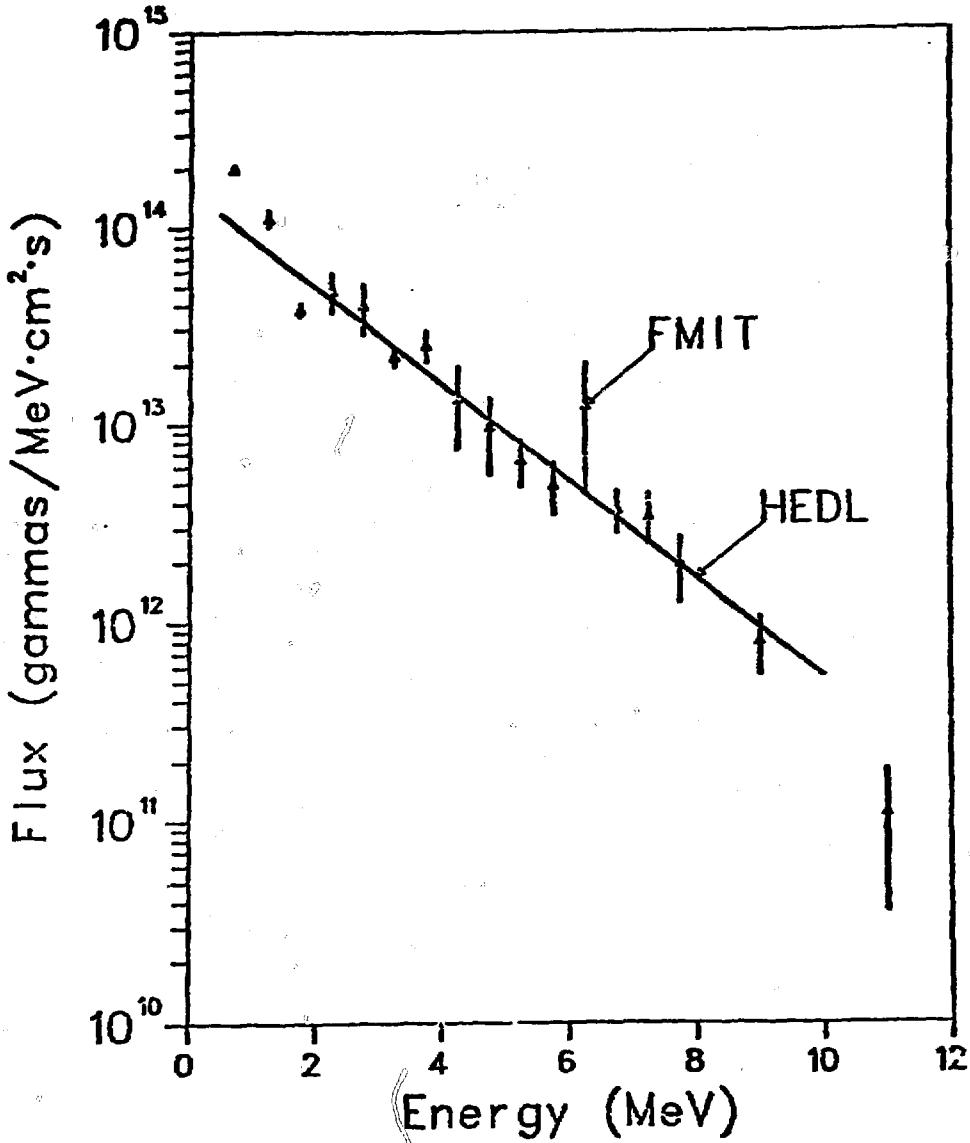
Flux (gammas/MeV·cm²·s)
10^15
10^14
10^13
10^12
10^11
10^10
0
2
4
6
8
10
12
Energy (MeV)
FMIT
HEDL

FIGURE 4